

MRI Contrast from Relaxation Along a Fictitious Field (RAFF)

T. Liimatainen¹, D. Sorce¹, M. Garwood¹, and S. Michaeli¹

¹Center for Magnetic Resonance Research, Dept. of Radiology, University of Minnesota, Minneapolis, MN, United States

Introduction: The trend towards higher magnetic field strengths (B_0) in NMR has been fueled mainly by the quest for increased signal-to-noise ratio. However, the laboratory frame longitudinal relaxation time (T_1), which is dominated by dipolar fluctuations occurring mainly near the Larmor frequency, $\omega_0 = \gamma B_0$ [1] is becoming less sensitive to slow molecular motions as B_0 increases. Relaxations in the presence of radiofrequency (RF) irradiation characterized by the rotating frame longitudinal and transverse relaxation time constants (T_{1p} and T_{2p} , respectively), can provide information about slow molecular motions at high magnetic fields. A practical limitation of rotating frame relaxation measurements is the relatively high RF power required by continuous-wave (cw) spin-lock, and adiabatic methods [2,3]. The high RF power requirement of the latter approach is a consequence of the need to satisfy the adiabatic condition, $|d\alpha/dt| \ll \omega_{eff}(t)$, where ω_{eff} is the rotating frame effective frequency (in units of angular velocity, $\omega_{eff}(t) = (\omega_0(t)^2 + (\Delta\omega(t))^2)^{1/2}$, with $\omega_0 = \gamma B_1$ and $\Delta\omega$ = offset frequency), and α is the time-dependent angle between the vector $\mathbf{B}_{eff}(t)$ and the laboratory frame z -axis. To reduce RF power requirements, we investigated the possibility of creating a time independent fictitious effective field (\mathbf{E}) generated under sub-adiabatic condition. We demonstrate theoretically that RAFF provides sensitivity to the slow rotational correlation times. Experiments on human brain demonstrate the potential of RAFF to generate contrast for MRI, while requiring less RF power than that typically used for T_{1p} and T_{2p} measurements. This new method is entitled relaxation along a fictitious field (RAFF).

Materials and Methods: The fictitious field is created by *sine* amplitude modulation $\omega_1(t) = \omega_1^{max} \sin(\omega_1^{max} t)$ and *cosine* frequency modulation $\Delta\omega(t) = \omega_1^{max} \cos(\omega_1^{max} t)$, where ω_1^{max} is the maximum amplitude of $\omega_1(t)$ leading to the condition $|d\alpha/dt| = \omega_{eff} = \text{constant}$. In the second rotating frame of reference, the amplitude of the \mathbf{E} is $E = (\omega_{eff}^2 + (d\alpha/dt)^2)^{1/2} = \text{constant}$, where $\alpha(t) = \tan^{-1}(\omega_1(t)/\Delta\omega(t))$. To overcome problems of RF inhomogeneity, a composite version of the pulse was designed (Fig. 1). The composite pulse follows BIR-4 scheme introduced earlier [4]. The theoretical calculations were carried out by applying second order perturbation theory [5] for dipolar interaction transformed to the ω_L -frame (relaxation along \mathbf{E}). Bloch simulations neglecting relaxation were used to investigate the evolution of magnetization (\mathbf{M}) during the *sine/cosine* pulse. All human experiments were carried out using a 4 T magnet (OMT, Inc., Oxon, UK) with Varian ^{UNITY}INOVA console (Varian Inc., Palo Alto, CA). Brains of healthy volunteers ($n=5$) were scanned using a volume TEM RF coil. Two measurements were conducted, with and without spin inversion (HS1, $T_p=10$ ms, $\omega_1^{max}/(2\pi) = 1.3$ kHz) prior to SC pulse,

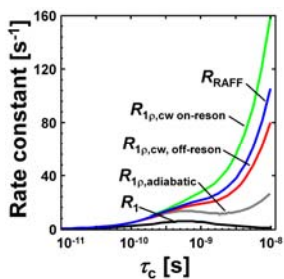


Fig. 2 Calculated longitudinal relaxation rate constants. The $R_{1p,E}$ (black) adiabatic R_{1p} (gray), on-resonance R_{1p} (green), off-resonance R_{1p} (red) with angle $\pi/4$, and $R_{1p,E}$ (blue) are presented. The on- and off-resonance R_{1p} using model given in [6] with $\omega_1^{max}/(2\pi) = 625$ Hz, adiabatic R_{1p} curves (HS1) was calculated according [2,6,7,8] and R_1 using model given in [6]. $\omega_1/(2\pi)$ of 200 MHz and $r = 158$ nm were used for all calculations.

$(\omega_1^{max}/(2\pi) = 625$ Hz, number of segments (2-64) leading to pulse train durations of 4.53-144.82 ms). Signal intensity decay and rise were measured with RAFF from one slice in the plane including *striatum* structures, using TurboFLASH imaging readout (TR/TE=10/5 ms, slice thickness = 3 mm). The fittings to data were performed using models

$$S_{+Z} = S_{0,+Z} \exp(-Rt) - S_{SS} (1 - \exp(-R_{SS}t)) \quad \text{and}$$

$S_{-Z} = S_{0,-Z} \exp(-Rt) - S_{SS} (1 - \exp(-R_{SS}t))$ for decaying and rising signal intensities. Here S_{+Z} and S_{-Z} are measured signals with and without the prior spin inversion, S_0 is the signal intensity before the RAFF weighting and S_{SS} the level of steady state with corresponding relaxation rates R and R_{SS} , respectively.

Results and Discussion: The sensitivity of the RAFF dipolar rate constant $R_{1p,E}$ for the change of the correlation times is demonstrated in Fig. 2, being close to that obtained by on-resonance continuous wave spin-lock $R_{1p} = R_2$. An intriguing property of RAFF found by the theoretical calculations is that $R_{1p,E} \equiv R_{2p,E}$. Using Bloch simulations, \mathbf{M} was found to follow \mathbf{E} once placed along it initially (Fig. 3) showing a locking property of \mathbf{E} . Signal intensity was found to end up in the same steady state independently of flip angle prior to the *sine/cosine* pulse in 5 mM GD-DTPA solution (data not shown). This suggests the necessity to use of the steady state analysis for the human RAFF relaxation time mapping. The relaxation time constants in the human brain were shown to be $\approx 20\%$ shorter when steady state fitting (Fig. 4a) was compared to mono-exponential fitting (Fig. 4c). The fraction SS ($=S_{SS}/S_0$) represents the contribution of steady state to RAFF and varied in mid brain areas, providing potential contrast (Fig. 4b). The average RF power delivered into the brain tissue during RAFF per unit time is 83 % of the adiabatic T_{1p} (HS1 pulses, $\omega_1^{max}/(2\pi) = 1.3$ kHz) and 61 % compared to continuous wave pulse with equal power with RAFF. The lower power requirement of RAFF as compared to adiabatic and continuous wave techniques may enable the use of RAFF contrast also in deep body structures where external RF power delivery is challenging for high field human applications.

References: [1] A.E. Bydder et al., Clinical Magnetic Resonance John Wiley&Sons 1980. [2] Michaeli et al., JMR 181 (2006) 135-147, [3] S. Michaeli et al., MRM 53 (2005) 823-829. [4] M. Garwood JMR A 112 (1995) 272-274. [5] A. Abragam Principles of Nuclear Magnetism. Oxford University Press Inc. 1963. [6] J. Blicharski, Acta Physica Polonica A41 (1972) 223-236. [7] M. Garwood, L. DelaBarre, JMR 153 (2001) 155-177. [8] S. Michaeli et al., JMR 169 (2004) 293-299.

The authors gratefully acknowledge financial support from: Instrumentarium Science Foundation (TL), Orion Corporation Research Foundation (TL), Finnish Cultural Foundation Northern Savo (TL), P30 NS057091, BTRR P41 RR008079, NIH R01NS061866 and NIH R21NS059813.

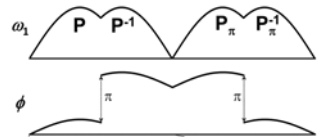


Fig. 1 Amplitude and phase modulations of RAFF pulse segment. P^1 is time-reverse of the P and π in sub-index designates π phase difference.

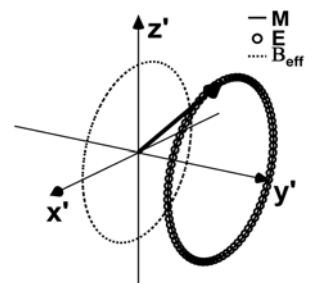


Fig. 3 Magnetization (\mathbf{M}) trajectory (solid line), calculated \mathbf{E} field (\circ) and \mathbf{B}_{eff} field (dotted line) during *sine/cosine* pulse in the ω_{RF} -frame. The evolution of initial \mathbf{M} along \mathbf{E} (thick arrow) was calculated using Bloch equations during one *sine/cosine* period.

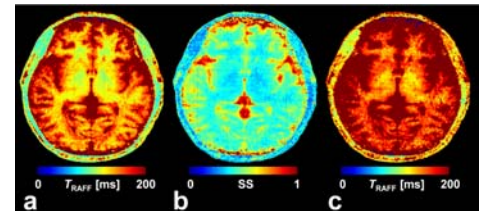


Fig. 4 a) RAFF relaxation time map obtained taking into account steady state b) corresponding steady state map and c) relaxation time map obtained using single mono-exponential fitting.